Bioactive Materials 39 (2024) 302–316

Contents lists available at ScienceDirect

Bioactive Materials

journal homepage: www.keaipublishing.com/en/journals/bioactive-materials

Netrin-1 co-cross-linked hydrogel accelerates diabetic wound healing in situ by modulating macrophage heterogeneity and promoting angiogenesis

Futing Shu [a,1], Hongchao Huang [a,1], Shichu Xiao [a,***], Zhaofan Xia [a,b,**], Yongjun Zheng [a,*]

[a] Department of Burn Surgery, The First Affiliated Hospital of Naval Medical University, Shanghai, 200433, People's Republic of China
[b] Research Unit of Key Techniques for Treatment of Burns and Combined Burns and Trauma Injury, Chinese Academy of Medical Sciences, Shanghai, 200433, People's Republic of China

ARTICLE INFO

Keywords:
Netrin-1
GelMA hydrogel
Diabetic wound healing
Angiogenesis
Macrophage heterogeneity

ABSTRACT

Diabetic wounds, characterized by prolonged inflammation and impaired vascularization, are a serious complication of diabetes. This study aimed to design a gelatin methacrylate (GelMA) hydrogel for the sustained release of netrin-1 and evaluate its potential as a scaffold to promote diabetic wound healing. The results showed that netrin-1 was highly expressed during the inflammation and proliferation phases of normal wounds, whereas it synchronously exhibited aberrantly low expression in diabetic wounds. Neutralization of netrin-1 inhibited normal wound healing, and the topical application of netrin-1 accelerated diabetic wound healing. Mechanistic studies demonstrated that netrin-1 regulated macrophage heterogeneity via the A2bR/STAT/PPARγ signaling pathway and promoted the function of endothelial cells, thus accelerating diabetic wound healing. These data suggest that netrin-1 is a potential therapeutic target for diabetic wounds.

1. Introduction

As a global epidemic affecting over 10.5 % of the world's adult population, diabetes has become a major health threat, causing numerous complications [1]. Research has shown that 25 % of patients with diabetes develop diabetic wounds in their lifetime, which has remained a significant challenge in the tissue repair field [2]. Although many therapies, including surgical debridement, infection control, dressing changes, and wound offloading, are available, the prognosis of diabetic wounds remains far from satisfactory [3]. Wound healing is a complex process comprising interdependent and overlapping stages, including hemostasis, inflammation, proliferation, and remodeling [4]. In diabetic wounds, all these events lose their physiological cascade and synchrony due to the sustained hyperglycemic environment, resulting in a prolonged inflammatory phase and impaired vascularization [5,6]. Further exploration of the pathogenesis of diabetic wounds and the development of a novel therapeutic approach to modulate the immune microenvironment and promote angiogenesis, are of great significance for diabetic wound healing.

Netrin-1, a diffusible laminin-like secreted protein, was initially identified as a guide for axonal migration and neuronal growth during embryonic development [7]. Recent studies have revealed that netrin-1 is extensively engaged in regulating organogenesis, tumorigenesis, inflammation, angiogenesis, and tissue remodeling [8–13]. It has been reported that Netrin-1 promoted the chronic inflammation in atherosclerosis by inactivating the emigration of macrophages from plaques [14]. However, the inflammation following ischemia/reperfusion injury in liver was resolved by exogenous netrin-1 upon binding to the adenosine receptor A2b (A2bR) [15]. Netrin-1 plays dual activities in angiogenesis as well. It has been well established that netrin-1 can be an angiogenic factor by binding to CD146 or an angiogenesis inhibitor when involving the UNC5B receptor [11,16,17]. Given the reported role of netrin-1 in inflammation and angiogenesis, we hypothesized that

Peer review under responsibility of KeAi Communications Co., Ltd.

* Corresponding author. Department of Burn Surgery, the First Affiliated Hospital of Naval Medical University, 168 Changhai Road, Yangpu District, Shanghai, 200433, People's Republic of China.
** Corresponding author. Department of Burn Surgery, the First Affiliated Hospital of Naval Medical University, 168 Changhai Road, Yangpu District, Shanghai, 200433, People's Republic of China.
*** Corresponding author. Department of Burn Surgery, the First Affiliated Hospital of Naval Medical University, 168 Changhai Road, Yangpu District, Shanghai, 200433, People's Republic of China.
E-mail addresses: huangzhuoxiao@sohu.com (S. Xiao), xiazhaofan_smmu@163.com (Z. Xia), smmuzhengyongjun@163.com (Y. Zheng).
[1] These authors contributed equally to this article.

https://doi.org/10.1016/j.bioactmat.2024.04.019
Received 20 January 2024; Received in revised form 16 April 2024; Accepted 18 April 2024

Abbreviations

BMDM	bone marrow-derived macrophage
DEG	differentially expressed gene
ELISA	enzyme-linked immunosorbent assay
GO	Gene Ontology
KEGG	Kyoto Encyclopedia of Genes and Genomes
HE	hematoxylin and eosin
HUVEC	human umbilical vein endothelial cell
HFB	human fibroblast
PPAR	peroxisome proliferator-activated receptor
SD	standard deviation
SEM	scanning electron microscope

netrin-1 is also be involved in the regulation of diabetic wound healing.

In this study, we aimed to explore the role of netrin-1 in diabetic wound healing. First, the expression profiles of netrin-1 were determined, and a neutralizing antibody against netrin-1 was intravenously administered to mice to explore the effect of netrin-1 on normal wound healing. Subsequently, *in vitro* and *in vivo* experiments were conducted to investigate the effect of netrin-1 on diabetic wound healing, mainly focusing on inflammation and angiogenesis of diabetic wounds. To further explore the efficacy of local netrin-1 administration, recombinant netrin-1 protein was coated into a gelatin methacrylate (GelMA) hydrogel to achieve sustained protein release. The primary goal of this project is to find a novel target for diabetic wound healing.

2. Materials and methods

2.1. Cell culture

The human umbilical vein endothelial cells (HUVECs) in our study were obtained from ScienCell Research Laboratories (San Diego, CA, USA) and cultured as previously described [3]. Human fibroblasts (HFBs) were isolated from human foreskin and cultured according to our previous research [18]. Bone marrow-derived macrophages (BMDMs) were prepared as previously described [3]. Briefly, bone marrow cells flushed from the femurs of 4-week-old C57BL/6 mice were seeded in 6-well plates (1×10^6/well) within RPMI Medium 1640 (Gibco, USA) supplemented with 10 % fetal bovine serum (Gibco) and 20 ng/mL M-CSF (Peprotech, USA). Cells were harvested on day 6 to identify macrophages using flow cytometry (Beckman Coulter, CA, USA) with FITC-conjugated anti-CD11b (0.25–0.5 μg/test, BD, USA) and APC-conjugated anti-F4/80 (2 μg/test, eBioscience, USA) antibodies, with the relevant isotype antibodies as the control. $F4/80^+CD11b^+$ cells were considered to be successfully induced macrophages. All cells in passages 2–5 were used for further experiments. The cells were cultured in high-glucose (HG) Dulbecco's modified Eagle medium (35 mmol/L) for at least 7 days, to simulate the hyperglycemic environment *in vivo*.

2.2. Flow cytometry

Qualified macrophages treated by Netrin-1 (125 ng/mL, 250 ng/mL, 500 ng/mL) were detached using 0.25 % trypsin-EDTA (Gibco) and incubated with APC-conjugated anti-CD206 antibody (BD) with the isotype antibody as the control. After washed by phosphate-buffered saline (PBS), the cell suspension was detected and the percentage of cells with the macrophage phenotype was analyzed using flow cytometry (Beckman Coulter).

2.3. Cell immunofluorescence

Macrophages were fixed in 4 % paraformaldehyde for 20 min and subsequently incubated with anti-CD206 antibody (Abcam, USA) overnight at 4 °C, followed by incubation with the corresponding secondary antibody (Thermo Fisher Scientific, USA) and DAPI staining (Beyotime, China). A fluorescence microscope (Olympus, Tokyo, Japan) was used to capture the images.

2.4. Cell migration assay

Cell migratory capacity was evaluated using scratch and Transwell assay. HUVECs reaching 90 % confluence in a 6-well plate were scratched with a pipette tip and cultured under the designated treatment. Mitomycin C was added to eliminate the impact of cell proliferation on the scratch closure [19]. Images were captured at the preset times using a light microscope (Olympus), and Image J software (NIH, USA) was employed to calculate the migration rates. For Transwell assay, 100 μL serum-free cell suspension (1×10^6/mL) was put into the upper chamber with the designed treatment in the lower chamber. After culturing in a cell incubator for 24 h, Transwell inserts were fixed with 4 % paraformaldehyde and stained with 0.1 % crystal violet. An optical microscope (Olympus) was used to capture images after wiping the cells in the upper chamber and Image J (NIH) was applied to perform quantitative analysis.

2.5. Cell proliferation assay

Cell proliferation was evaluated using Cell Counting Kit-8 (CCK-8, Dojindo, Japan). Briefly, cells (5×10^4/mL) suspended in the desired treatment were added into 96-well plates. When reaching the preset time points, the cells were incubated with 100 μL CCK-8 working solution at 37 °C for 2 h. The optical density at 450 nm was measured by a microplate reader (SpectraMax M4, CA, USA).

2.6. Capillary tube formation

Matrigel matrix (60 μL, Corning, USA) was put into a 96-well plate and incubated at 37 °C for solidification. Cell suspension of HUVECs (100 μL, 5×10^5 cells/mL) under the designed treatment was added to form the capillary tubes. Tube images were captured with an optical microscope (Olympus) and analyzed by the angiogenesis analyzer in Image J software (NIH).

2.7. Western blotting analysis

Total protein was obtained using a RIPA lysis buffer (Servicebio, China) containing protease/phosphatase inhibitors (NCM Biotech, China) and the protein concentration was assessed using a BCA Protein Assay Kit (Thermo Fisher Scientific, USA). In brief, 20 μg protein per sample was loaded and separated by SDS-PAGE and then electrotransferred onto a polyvinylidene fluoride membrane. After blocking with a 5 % non-fat milk solution, the membranes were incubated overnight at 4 °C with primary antibodies, followed by the

Table 1
Antibodies utilized in Western blotting.

Antibodies	Company	Catalog Number	Concentration
GAPDH	Engibody	AT0002	1:2000
Netrin-1	Enzo	ALX-804-838-C100	1:1000
Collagen I	Abcam	ab260043	1:1000
Collagen III	Invitrogen	PA5-27828	1:1000
α-SMA	Abcam	ab7817	1:3000
CD86	Santa Cruz	sc-28347	1:1000
CD206	Abcam	ab64693	1:1000
STAT3	Abcam	ab68153	1:1000
pSTAT3	CST	94994 T	1:1000
STAT6	Abcam	ab32520	1:1000
pSTAT6	Abcam	ab263947	1:1000
PPARγ	Abcam	ab45036	1:500

corresponding secondary antibodies at room temperature for 1 h (Table 1). The bands were detected using enhanced chemiluminescent substrates (Thermo Fisher Scientific) and evaluated quantitatively using Image J software (NIH).

2.8. Quantitative reverse transcription-polymerase chain reaction (RT-qPCR)

Total RNA was extracted using a TRIzol reagent (Life Technologies, USA) and reverse-transcribed to synthesize cDNA using a PrimeScriptTMRT Master Mix (TaKaRa, Japan). Then, a StepOnePlus Real-Time PCR System (Applied Biosystems, USA) was used to amplify cDNA with an SYBR Premix Ex Taq™ kit (TaKaRa). Using the primer sequences presented in Table 2, the mRNA levels of target genes were quantified and normalized to that of β-actin.

2.9. RNA sequencing (RNA-seq) analysis

Macrophages were stimulated with tumor necrosis factor (TNF)-α and interferon (IFN)-γ (20 ng/mL each, Peprotech) combined with recombinant netrin-1 protein (500 ng/mL, R&D, USA) for 48 h. Total RNA was harvested using a TRIzol reagent (Life Technologies) and sent to Novogene Company (Shanghai, China) for the following processes. Eukaryotic mRNA was first enriched using oligo (dT) magnetic beads and converted into individual cDNA libraries. RNA-seq was then performed using Illumina technology (San Diego, CA, USA) to screen for differentially expressed genes (DEGs) with the thresholds of $|\log2 \text{ fold change}| > 0$ and $P < 0.05$, followed by Gene Ontology (GO) enrichment and Kyoto Encyclopedia of Genes and Genomes (KEGG) pathway analyses.

2.10. Preparation of GelMA, GelMA/NTN1 and GelMA-c-NTN1

GelMA, a lithiumphenyl-2,4,6-trimethylbenzoyl phosphinate (LAP) photo-initiator, and acrylate-PEG-NHS (AC-PEG-NHS) were purchased from Engineering for Life Co., Ltd (Suzhou, China). According to the manufacturer's instruction, netrin-1 (R&D) dissolved in a 0.25 % LAP photo-initiator standard solution was PEGylated with AC-PEG-NHS for 24 h. A sterile 10 % GelMA precursor solution was generated following the manufacturer's protocol. GelMA-*c*-NTN1 was made with GelMA solution and PEGylated netrin-1 at the desired netrin-1 concentration of 20 μg/mL. For GelMA/NTN1, the equal non-covalently entrapped netrin-1 was added to the GelMA solution. The GelMA, GelMA/NTN1 and GelMA-*c*-NTN1 hydrogels were harvested after chemical cross-linking with UV light (405 nm) for 10 s.

2.11. Characterization of hydrogels

After lyophilization and gold spraying, the morphologies of GelMA and GelMA-*c*-NTN1 hydrogel samples were observed and photographed using a scanning electron microscope (SEM, Zeiss sigma 300, Carl Zeiss, Germany). GelMA and GelMA-*c*-NTN1 hydrogels were prepared and immersed in PBS at 37 °C for 48 h, with their initial weights recorded as W0 and those at preset time points (1, 3, 6, 12, 24, 48 h) Wt accordingly. The swelling rate was calculated as follows: swelling ratio = (Wt - W0)/W0 × 100 %. For the tensile assay, an electronic universal testing machine (Instron, USA) was employed to stretch the crosslinked GelMA and GelMA-*c*-NTN1 hydrogels at a speed of 1 mm/min and the stress-strain curve was recorded until the scaffold was broken. For the degradation assay, all scaffolds were immersed in PBS at 37 °C and the remaining masses were weighted at the predetermined time points to track the degradation kinetics. The GelMA/NTN1 and GelMA-*c*-NTN1 hydrogels were kept in PBS at 37 °C, and the supernatant was collected after 2, 4, 7, and 14 days to examine the protein level using a mouse netrin-1 ELISA kit (CUSABIO, China). The protein release ratio was calculated with the detected netrin-1 levels in the PBS and the initial loading.

Table 2
Primer sequences for RT-qPCR.

Gene	Forward (5' – 3')	Reverse (5' – 3')
mCD86	GCACGGACTTGAACAACCAG	CCTTTGTAAATGGGCACGGC
mTNFα	CCCTCACACTCAGATCATCTTCT	GCTACGACGTGGGCTACAG
mIL1β	GAAATGCCACCTTTTGACAGTG	CTGGATGCTCTCATCAGGACA
mIL 6	TAGTCCTTCCTACCCCAATTTCC	TTGGTCCTTAGCCACTCCTTC
mCD206	GAGGGAAGCGAGAGATTATGGA	GCCTGATGCCAGGTTAAAGCA
mARG 1	GAATCTGCATGGGCAACCTGTGT	AGGGTCTACGTCTCGCAAGCCA
mIL 10	GCTCTTACTGACTGGCATGAG	CGCAGCTCTAGGAGCATGTG
mVEGF	GCACATAGAGAGAATGAGCTTCC	CTCCGCTCTGAACAAGGCT
mβ-actin	GGCTGTATTCCCCTCCATCG	CCAGTTGGTAACAATGCCATGT

2.12. Cell viability and morphology

Cell viability was assessed using a Live/dead Kit (Invitrogen, USA) in accordance with the manufacturer's instruction. Briefly, HFBs were cultured for 24 h in a 96-well plate pre-coated with GelMA, GelMA/NTN1 and GelMA-*c*-NTN1 hydrogels, and then incubated with a Live/dead working solution for 30 min. Cell morphology was observed via cytoskeletal staining with fluorescein isothiocyanate (FITC)-phalloidin (Abcam) with cellular nuclei counterstained with DAPI (Beyotime). The stained cells were photographed using a fluorescence microscope (Olympus) and the images were processed with Image J software (NIH).

2.13. In vivo wound healing performance

All animal protocols followed the guidelines of the Animal Ethics Committee of the First Affiliated Hospital of Naval Medical University. C57BL/6 mice, db/db mice and db/m littermate (male, 8–10 weeks old) in this research were all purchased from GemPharmatech Co., Ltd. (Jiangsu, China). The blood glucose levels of db/db mice were all >300 mg/dL. First, all mice were anesthetized with isoflurane and their dorsal hair was shaved by an electric razor. The dorsal skin was further depilated with a depilatory cream and then disinfected with alcohol. Two full-thickness cutaneous wounds were generated on the dorsum on each side of midline, using a sterile 8-mm diameter biopsy punch. All wounds were cleaned, photographed and changed dressings every 3 days until completely healed. The wound healing rates were calculated using ImageJ software (NIH) by the following formula: wound closure (%) = (A0 − At)/A0 × 100 % (A0: the wound area on day 0, At: the wound area without epithelization at time t).

Normal wounds were established with C57BL/6 mice and randomly harvested at the preset schedule (days 0, 3, 6, and 9) to track netrin-1 expression. To verify the role of netrin-1 in normal wound healing, the mice were randomly divided into two groups after the normal wounds were induced. Mice in the experimental group were injected via the tail vein with mouse netrin-1-neutralizing antibody (10 mg/kg, AF1109, R&D Systems) on days 3 and 6, with the control mice injected with the isotype antibody (10 mg/kg, AB108C, R&D Systems) [9,20].

Similarly, db/db mice and their db/m littermates were used to establish wounds, and the samples were collected to detect the sequential expression of netrin-1. To explore the function of netrin-1 protein, diabetic wounds were generated using db/db mice, which were randomly divided into the netrin-1 treatment and control groups. Netrin-1 protein (20 μg/mL, 50 μL per wound) was then injected intradermally around the wound on days 3 and 6, with the PBS injected as the control. To further investigate the effect of GelMA-*c*-NTN1 on wound healing, the diabetic wounds were covered with the sterilized GelMA, GelMA/NTN1 and GelMA-*c*-NTN1 hydrogels crosslinked via UV-irradiation (50 μL per wound) on day 3.

2.14. Histological and immunofluorescence staining analysis

The harvested wound samples were fixed in 4 % paraformaldehyde,

embedded in paraffin, and then cut into 8 μm-thick sections. Hematoxylin and eosin (HE), Masson's trichrome staining and Sirius Red staining were performed to observe the histological structure and collagen components of the wound samples. In addition, immunohistochemical staining was conducted using primary antibodies against CD31 (Abcam) and Ki67 (Abcam) to evaluate wound angiogenesis and cell proliferation. Immunofluorescence staining with antibodies against netrin-1 (Enzo, USA), CD31 (Abcam), F4/80 (Santa Cruz, USA) and CD206 (Abcam) was processed to track netrin-1 expression, evaluate angiogenesis and identify M2 macrophages in wounds. A microscope (Olympus) was used to observe the stained sections and the obtained images were analyzed by Image J (NIH).

2.15. Enzyme-linked immunosorbent assay (ELISA)

Cytokines in the wound microenvironment were quantitatively detected by ELISA. In brief, the supernatants collected from the wound tissues were pipetted into wells pre-coated with the corresponding antibodies and then incubated for 90 min. The wells after washed were added with an enzyme-linked specific antibody, followed by a substrate solution resulting in a color signal. The absorbance of the samples was measured by a microplate reader (SpectraMax M4), and cytokine levels were estimated using the standard curve.

2.16. Statistical analysis

All data were presented as the mean ± standard deviation (SD) and analyzed using GraphPad Prism 10.0 software (GraphPad, La Jolla, USA). Student's t-test was applied to compare two groups and one-way analysis of variance (ANOVA) was used among multi-group comparison. Data were considered statistically significant at $P < 0.05$ (*$P < 0.05$, **$P < 0.01$, ***$P < 0.001$, and ****$P < 0.0001$).

3. Results

3.1. Netrin-1 was indispensable in normal wound healing

In this study, C57BL/6 mice were used to establish a full-thickness skin defect. Western blotting revealed that netrin-1 protein exhibited high expressions in the wound sites on days 3 and 6 post wounding, while its expression decreased on day 9 without a significant difference compared to day 0 (Fig. 1A). To explore the role of netrin-1 in wound healing process, a mouse netrin-1 neutralizing antibody was intravenously administered on days 3 and 6 post-wounding to antagonize the function of netrin-1, showing that the wound healing was inhibited (Fig. 1B). HE and Masson's trichrome staining (Fig. 1D–E) presented that the control group achieved complete re-epithelialization with abundant collagen deposition in the wound bed on day 9. In contrast, the netrin-1 antagonism group exhibited obvious epidermal defects and wafery granulation tissue.

Macrophages, the main undertaker of the inflammatory stage, are crucial for initiating regenerative responses [4,21,22]. Immunofluorescence staining results in Fig. 1C showed that the control group had a significantly larger population of M2 macrophages ($F4/80^+CD206^+$ cells, 39.78 % ± 2.60 %) than the netrin-1 antagonism group (24.18 % ± 3.12 %, $P < 0.0001$) on day 6, suggesting that a lack of netrin-1 inhibited the transformation of macrophages from the M1 to the M2 phenotype. Moreover, immunohistochemical staining on day 9 post-wounding exhibited apparent fewer capillary vessels in the netrin-1 antagonism group than that in the control group (Fig. 1F–G). Furthermore, Sirius Red staining indicated that compared to the control group, collagen synthesis in the netrin-1 antagonism group was significantly weaker with less bundled collagen fibers (Fig. 1H–I). These results indicate that netrin-1 is highly expressed during the inflammation and proliferation phases and may serve as a potential important protein molecule in the wound healing process by regulating macrophage transition and wound vascularization.

3.2. Netrin-1 was aberrantly weakly expressed in diabetic wounds, and topical netrin-1 injection intradermally promoted diabetic wound healing

To further track the profile of netrin-1 expression during the healing process of diabetic and normal wounds, full-thickness skin defects were created in db/db and db/m mice. The results showed that the diabetic wounds healed significantly slower than the normal wounds (Fig. 2A). Immunofluorescence staining for netrin-1 exhibited that netrin-1 expression in diabetic wounds remained abnormally low on days 3 and 6 post-wounding (Fig. 2B).

To explore the role of netrin-1 in diabetic wound healing, recombinant netrin-1 protein was injected intradermally into the wound edges on days 3 and 6. The preliminary experiments presented in Fig. S1 have shown that 20 μg/mL netrin-1 (50 μL per wound) was the minimum to achieve the greatest wound healing efficacy and selected as the optimal therapeutic dosage in this study. The results in Fig. 2C showed that the wound healing process was significantly promoted, with a healing rate of 97.24 % ± 1.86 % on day 9 in the netrin-1 treated group and 62.58 % ± 9.58 % in the control group. HE staining showed that the wound bed was fully epithelialized with the abundant granulation tissue on day 9 in the netrin-1 injection group, whereas the control group still presented a visible wound with thin granulation tissue (Fig. 2F). Further immunofluorescence staining revealed that the M2 macrophage population ($F4/80^+CD206^+$ cells) was significantly increased after treatment with recombinant netrin-1 protein (Fig. 2D). Consistent with the macrophage immunofluorescence results, ELISA detection showed that the expression of representative inflammatory cytokines (TNF-α, IL-1β, and IL-6) significantly reduced in the netrin-1-treated group, while that of typical growth factors (TGF-β1, IGF-1, and VEGF-A) evidently increased (Fig. 2E).

As wound inflammation gradually subsides, wound repair enters the granulation tissue formation stage, characterized by cell proliferation, angiogenesis, and collagen synthesis [4,23]. Immunohistochemical staining revealed that the number of $Ki67^+$ cells was significantly higher in the netrin-1 group than that in the control group (Fig. 2G). Images of the wound base showed the dense and interwoven blood vessels with the apparent granulation tissue in the netrin-1 group, in contrast, only a few blood vessels were visible in the control group (Fig. 2H). These results were further supported by immunohistochemical staining, which showed more $CD31^+$ vessels in the netrin-1-treated group (Fig. 2I). Moreover, Sirius Red staining showed increased collagen deposition with tightly arranged orange-red thick fibers upon netrin-1 treatment (Fig. 2J). Western blotting demonstrated that netrin-1 treatment significantly enhanced the synthesis of collagen I, collagen III, and α-SMA in diabetic wounds (Fig. 2K).

Taken together, the expression of netrin-1 is low in diabetic wounds. However, local application of netrin-1 could promote the healing of diabetic wounds partially by regulating macrophage polarization and neovascularization.

3.3. Netrin-1 regulated macrophage polarization via the A2bR/STAT/PPARγ signaling pathway in vitro

Primary BMDMs were extracted and cultured referring to Fig. 3A, and identified using flow cytometry. The results in Fig. 3B indicated that the population of $F4/80^+CD11b^+$ cells was up to 98.42 %, showing the high purity of the induced macrophages in this study. Subsequently, macrophages were stimulated with TNF-α and IFN-γ to achieve classical macrophage activation [24]. Microscopy images in Fig. 3C revealed that upon TNF-α and IFN-γ stimulation, macrophages exhibited a circular shape with dendritic protrusions, whereas their morphology elongated when netrin-1 protein was added. Flow cytometry results showed that the proportion of $CD206^+$ macrophages increased after treatment with different concentrations of netrin-1 protein (Fig. 3D). This finding was

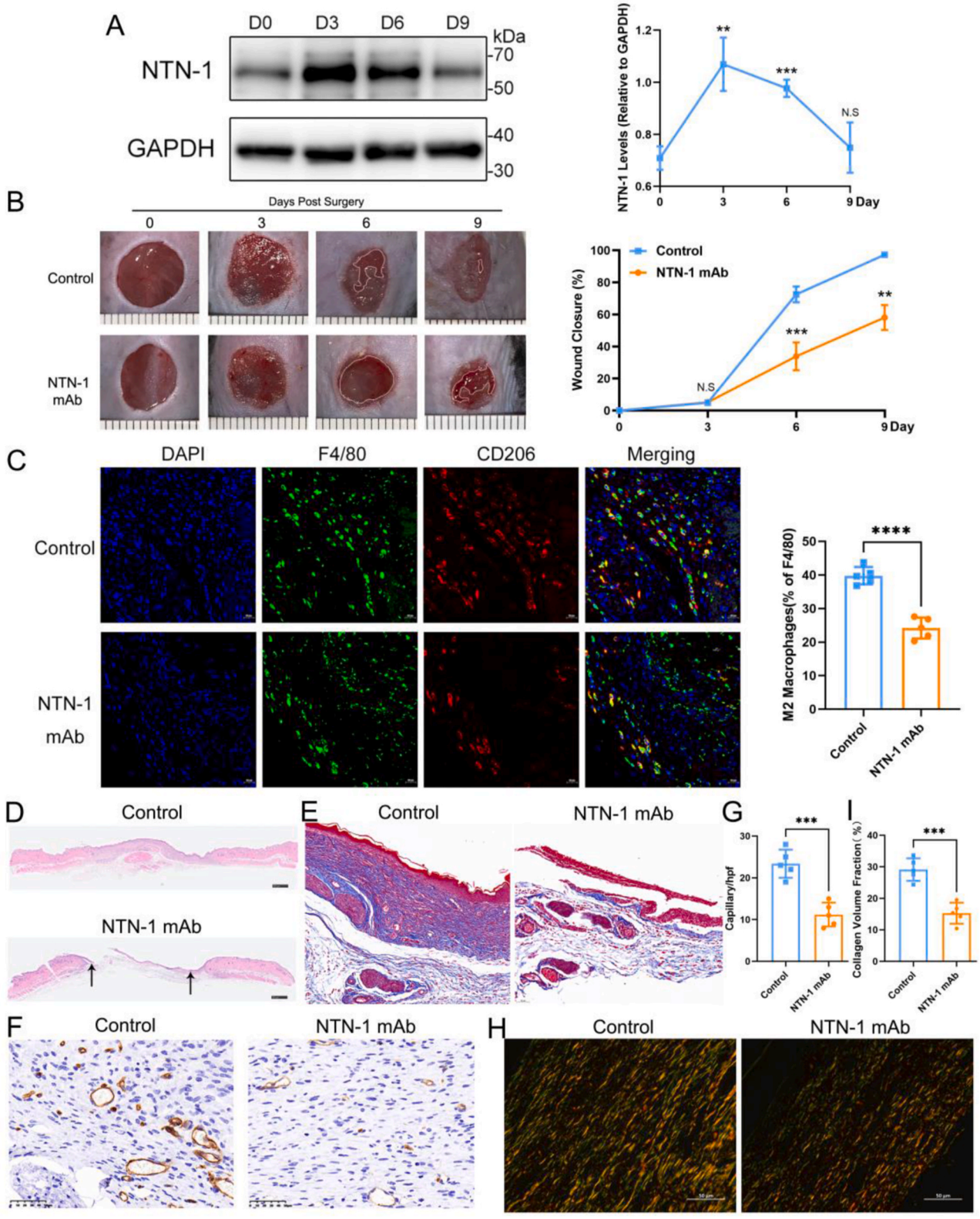

Fig. 1. Netrin-1 was indispensable in normal wound healing. (A) Western blotting of netrin-1 expression on days 0, 3, 6, and 9 post-wounding (compared to day 0, n = 3). (B) Images of normal wounds after treatment with NTN-1 mAb and the statistical analysis of the wound healing rates (%) (n = 4). (C) Immunofluorescence staining of F4/80 (green) and CD206 (red) showing the accumulation of M2 macrophages on day 6 post-wounding (scale bar: 20 μm, n = 5). (D) Hematoxylin and eosin staining on day 9 post-wounding (scale bar: 500 μm, black arrows indicate the wound edges). (E) The presentative images of Masson's trichrome staining (scale bar: 50 μm). (F–G) Immunohistochemistry staining of CD31 with the corresponding statistical data (scale bar: 50 μm, n = 5). (H–I) Sirius Red staining with an analysis of collagen volume (scale bar: 50 μm, n = 5). Netrin-1, NTN-1. Netrin-1 monoclonal antibody, NTN-1 mAb. Data are shown as the mean ± SD. **P < 0.01, ***P < 0.001, ****P < 0.0001, and N·S, no significance.

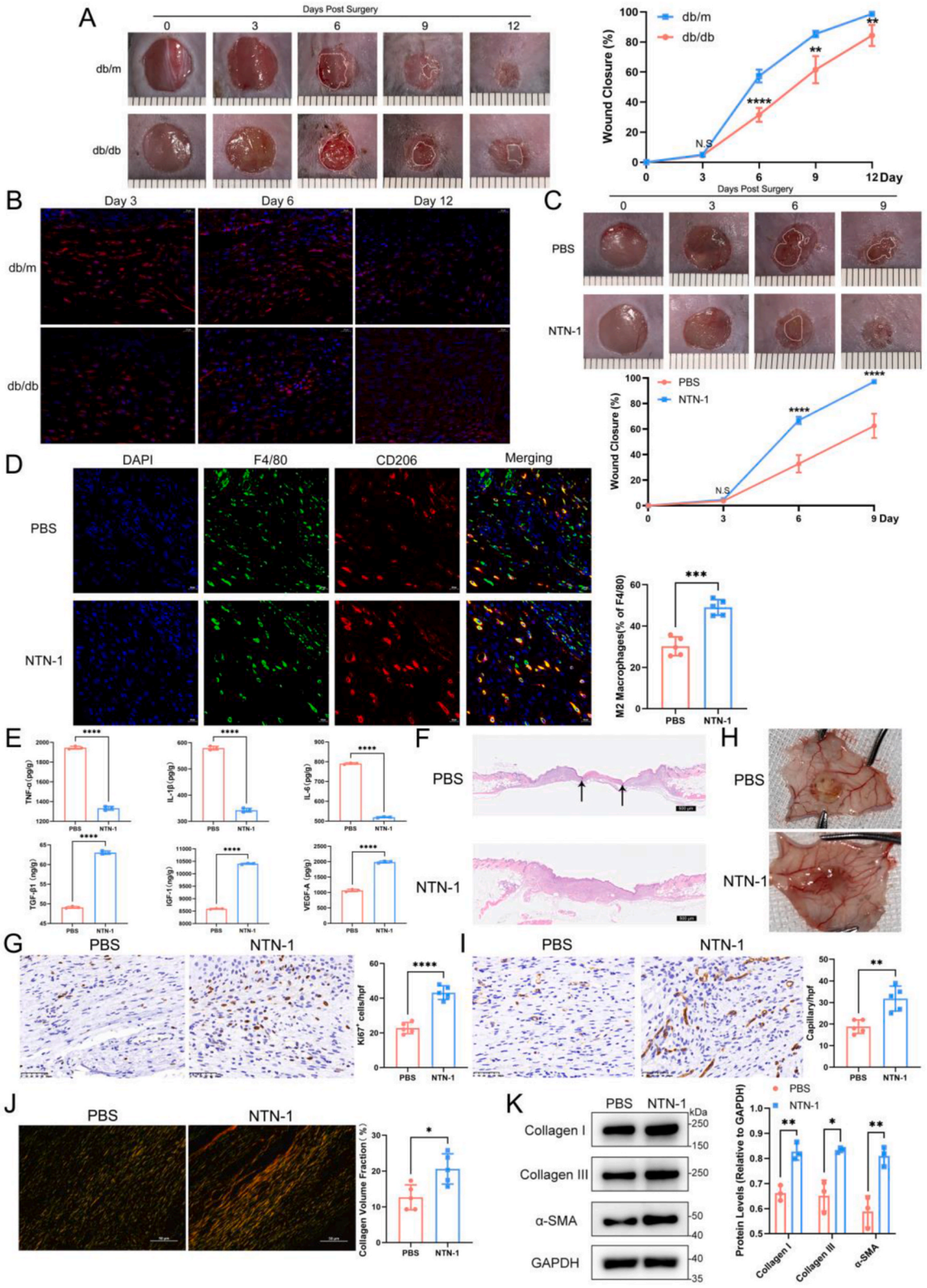

Fig. 2. Expression profile of netrin-1 was aberrantly low in diabetic wounds, and topical netrin-1 injection intradermally promoted diabetic wound healing. (A) Images of normal and diabetic wounds and the statistical analysis of the wound healing rates (%) (n = 5). (B) Immunofluorescence staining for netrin-1 (scale bar: 20 μm). (C) Images of diabetic wounds after treatment with netrin-1 and the statistical analysis of the wound healing rates (%) (n = 5). (D) Immunofluorescence staining of F4/80 (green) and CD206 (red) showing the accumulation of M2 macrophages on day 6 post-wounding (scale bar: 20 μm, n = 5). (E) ELISA analysis of inflammatory cytokines (TNF-α, IL-1β, and IL-6) and growth factors (TGF-β1, IGF-1, and VEGF-A) on day 6 post-wounding (n = 3). (F) Hematoxylin and eosin staining of the wounds on day 9 post-wounding (scale bar: 500 μm, black arrows indicated wound edges). (G and I) Immunohistochemistry staining of Ki67 and CD31 with the statistical data (scale bar: 50 μm, n = 5). (H) Representative images of the wound base on day 9 post-wounding. (J) Sirius Red staining results and an analysis of the collagen volume (scale bar: 50 μm, n = 5). (K) Western blotting of collagen I, collagen III, and α-SMA expression in the wound sites, including quantitative measurements (n = 3). Netrin-1, NTN-1. Data are shown as the mean ± SD. *P < 0.05, **P < 0.01, ***P < 0.001, ****P < 0.0001, and N·S, no significance.

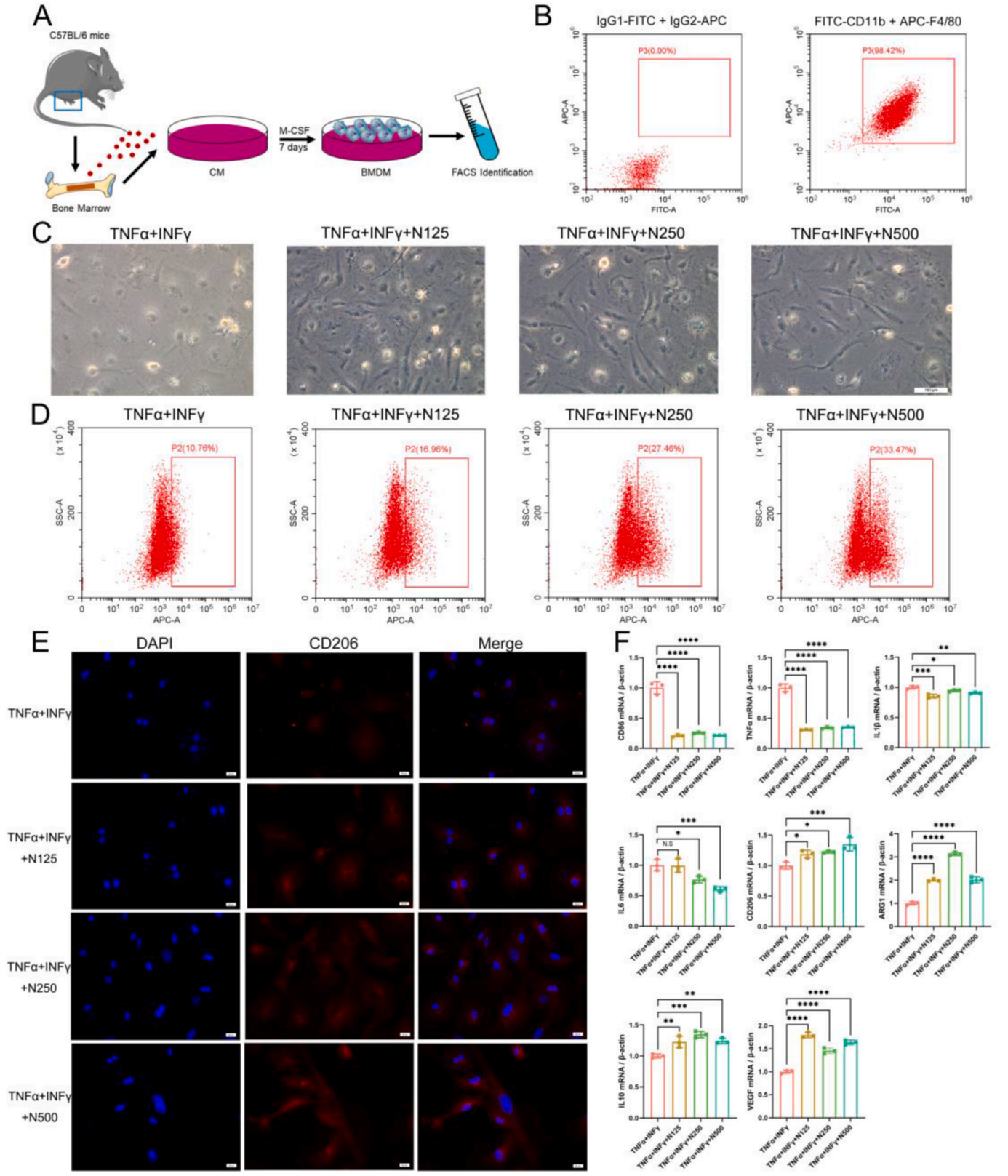

Fig. 3. Netrin-1 could promote the switch of macrophages toward the M2 phenotype and modulate cellular functions *in vitro*. (A) Procedures for bone marrow-derived macrophage (BMDM) preparation. (B) FACS of $CD11b^{+}$ and $F4/80^{+}$ cell populations (%) in the induced bone marrow-derived cells. (C) Changes in macrophage morphology after treatment with netrin-1 (scale bar: 100 μm). (D) Flow cytometry analysis of $CD206^{+}$ macrophages upon netrin-1 treatment. (E) Immunofluorescence staining of CD206 showing the existing M2 macrophages (scale bar: 20 μm). (F) RT-qPCR analysis of macrophage markers (M1: CD86, TNF-α, IL-1β, and IL-6; M2: CD206, ARG1, IL-10, and VEGF) in netrin-1-treated BMDMs (n = 3). Netrin-1 (125 ng/mL), N125; netrin-1 (250 ng/mL), N250; netrin-1 (500 ng/mL), N500. Fluorescence-activated cell sorting, FACS. Data are shown as the mean ± SD. *P < 0.05, **P < 0.01, ***P < 0.001, ****P < 0.0001, and N·S, no significance.

further confirmed by immunofluorescence staining for CD206 expression in macrophages (Fig. 3E). Moreover, RT-qPCR was performed to validate the phenotype and function of the macrophages. As shown in Fig. 3F, netrin-1 significantly inhibited the expression of M1 markers (CD86, TNF-α, IL-1β, and IL-6) and promoted the synthesis of M2 markers (CD206, ARG1, IL-10, and VEGF) in macrophages. These results indicate that netrin-1 could promote the switching of macrophages toward the M2 phenotype.

To further explore the mechanism underlying the wound-healing effects of netrin-1, the mRNA profile of macrophages treated with netrin-1 (500 ng/mL) under inflammatory stimulation was determined using RNA-seq analysis, identifying 640 DEGs. The volcano plot and histogram were shown in Fig. 4A and B, respectively. A heat map of macrophage markers revealed that stimulation with TNF-α and IFN-γ induced the high expression of M1 markers (such as CXCL16, NOS2, TNF, and IL1α) in macrophages, while treatment with TNF-α, IFN-γ and Netrin-1 promoted the upregulation of M2 markers (such as IL4, VEGF, CD14, and PPARγ) (Fig. 4C). GO (Fig. 4D) and KEGG (Fig. 4E) analyses further showed that the peroxisome proliferator-activated receptor (PPAR) signaling pathway, a classical pathway underlying macrophage polarization, was enriched. Next, GW9662 (a PPARγ-specific inhibitor) was used to verify the core role of this pathway in wound healing. Western blotting results of CD86 and CD206 expression implied that the role of netrin-1 in promoting M2 polarization was reversed by GW9662 (Fig. 4F). Furthermore, key proteins of the PPAR signaling pathway were detected, showing that netrin-1 significantly enhanced the expressions of pSTAT3, pSTAT6, and PPARγ in macrophages under an inflammatory environment (Fig. 4G). Previous studies have shown that A2bR, a classic receptor of netrin-1, was abundantly expressed in macrophages [25]. In this study, MRS (an A2bR antagonist) was added to macrophages, and the results demonstrated that the STAT/PPARγ pathway activated by netrin-1 was inhibited by MRS, indicating that netrin-1 may induce M2 macrophage polarization by binding to A2bR and activating the downstream STAT/PPARγ pathway. Immunofluorescence staining of CD206, a marker of M2 macrophages, confirmed the western blotting results (Fig. 4H–I). Further RT-qPCR analysis revealed that netrin-1 inhibited the expression of CD86, TNF-α, IL-1β, and IL-6 (M1 markers) and promoted that of CD206, ARG1, IL-10, and VEGF (M2 markers); these trends could be reversed by GW9662 or MRS treatment (Fig. 4J).

3.4. Netrin-1 promoted the angiogenic capability of endothelial cells in vitro

To investigate the effects of netrin-1 on endothelial cells, netrin-1 at concentrations of 0, 125, 250, and 500 ng/mL was added to HUVECs. The CCK8 assay results showed that netrin-1 slightly promoted the proliferation of endothelial cells (Fig. 5A). The scratch (Fig. 5B–C) and Transwell assays (Fig. 5D) demonstrated that netrin-1 significantly promoted HUVEC migration. Moreover, the tube formation assay revealed the formation of complete and irregular tube structures upon netrin-1 stimulation (Fig. 5E).

3.5. Characterization, biocompatibility, and bioactivity of GelMA-c-NTN1 hydrogels

To avoid injection pain and infection and prolong the biological activity of netrin-1 on wounds, we developed a netrin-1-wrapped hydrogel for topical administration. PEGylated netrin-1 was added to the GelMA precursor solution to form a mixed liquid with good fluidity, and the GelMA-*c*-NTN1 hydrogel was formed after irradiation with UV light (Fig. 6A). As observed via SEM, GelMA and GelMA-*c*-NTN1 both exhibited a continuous, irregular, and interconnected porous three-dimensional network structure (Fig. 6B). The swelling behaviors of GelMA and GelMA-*c*-NTN1 were similar (Fig. 6C). The stress-strain curve showed that the tensile strength of GelMA-*c*-NTN1 was slightly higher than that of GelMA, with GelMA-*c*-NTN1 and GelMA having elongations at break of 31.1 % and 26.2 %, respectively (Fig. 6D). The degradation tests in PBS indicated similar degradation rates for both hydrogels over time (Fig. 6E). In addition, ELISA was used to assess the protein release profile of the hydrogels. Slower protein release was observed from GelMA-*c*-NTN1 than that from GelMA/NTN1 (Fig. 6F). Cell viability (Fig. 6G) and morphology (Fig. 6H) analyses showed that GelMA and GelMA-*c*-NTN1 were non-cytotoxic. Furthermore, GelMA-*c*-NTN1 retained its efficacy in promoting endothelial cell tube formation (Fig. 6I).

3.6. GelMA-c-NTN1 hydrogel accelerated diabetic wound healing in vivo

A GelMA-*c*-NTN1 hydrogel was constructed to cover diabetic wounds (Fig. 7A). Representative images of the wounds were shown in Fig. 7B, and the comparable schematic diagrams of the wound areas were exhibited in Fig. 7C. Topical application of GelMA-*c*-NTN1 significantly accelerated wound closure in diabetic mice (Fig. 7D). HE staining was also performed to evaluate the wound structure on day 9. As shown in Fig. 7E, the wounds in the GelMA-*c*-NTN1 group achieved a completely continuous epidermal layer with more abundant granulation tissue than those in the other groups. Masson's trichrome staining and Sirius Red staining were used to determine the architecture of extracellular matrix, revealing that the more abundant and mature collagen deposited in the GelMA-*c*-NTN1 group (Fig. 7F7H). Moreover, immunofluorescence staining of CD31 was performed to evaluate the wound angiogenesis. As shown in Fig. 7G, GelMA-*c*-NTN1 covered wounds presented a significantly higher vascular density, compared with the other two hydrogels and the untreated wounds. The enhanced efficacy was due to the sustained released netrin-1, for no significant difference of wound repairing ability was observed between GelMA and GelMA-PEG hydrogel groups (Fig. S2).

4. Discussion

In this study, we demonstrated the potential contribution of netrin-1 toward delayed wound healing in diabetes. Topical netrin-1 administration accelerated wound repair in diabetic mice, partially by promoting macrophage polarization towards the M2 phenotype via the A2bR/STAT/PPARγ signaling pathway and enhancing the angiogenic capability of endothelial cells. We further developed a GelMA-*c*-NTN1 hydrogel to achieve the sustained release of netrin-1 and this may provide a novel therapeutic approach for diabetic wound closure (Fig. 8).

Accumulating evidence has positioned that macrophages adapt their conversion from pro-inflammatory macrophages towards the pro-healing phenotype upon spatiotemporal cues in the coordinated healing process, which generates a positive feedback loop to establish a favorable immune microenvironment and drive a progressive cell proliferative cascade [23,26–29]. However, the specific hyperglycemic environment in diabetic wounds impairs cellular response and stimulates macrophages to massively secrete inflammatory cytokines (such as TNF-α, IL-1β, and IL-6), encouraging the vicious cycle of maintaining the M1 macrophage phenotype and prolonging inflammation [22,30,31]. Therefore, promoting macrophage heterogeneity has become an active area of research for accelerating diabetic wound healing. There have been some reports on the involvement of netrin-1 in macrophage regulation, however, whether netrin-1 exhibits pro- or anti-inflammatory roles depends on the different settings [32]. A recent study showed that silencing netrin-1 can ameliorate atherosclerotic inflammation and promote plaque regression by alleviating macrophage retention and inducing pro-resolving macrophages in plaques [33]. In contrast, netrin-1 generated alternatively activated macrophages to attenuate renal and cardiac ischemia/reperfusion injury [34,35]. However, the relationship between netrin-1 and macrophages in wounds has not been reported. In this study, we found that netrin-1 was highly expressed on day 3 post-wounding, and that macrophage polarization was impaired after netrin-1 inhibition using neutralizing antibody,

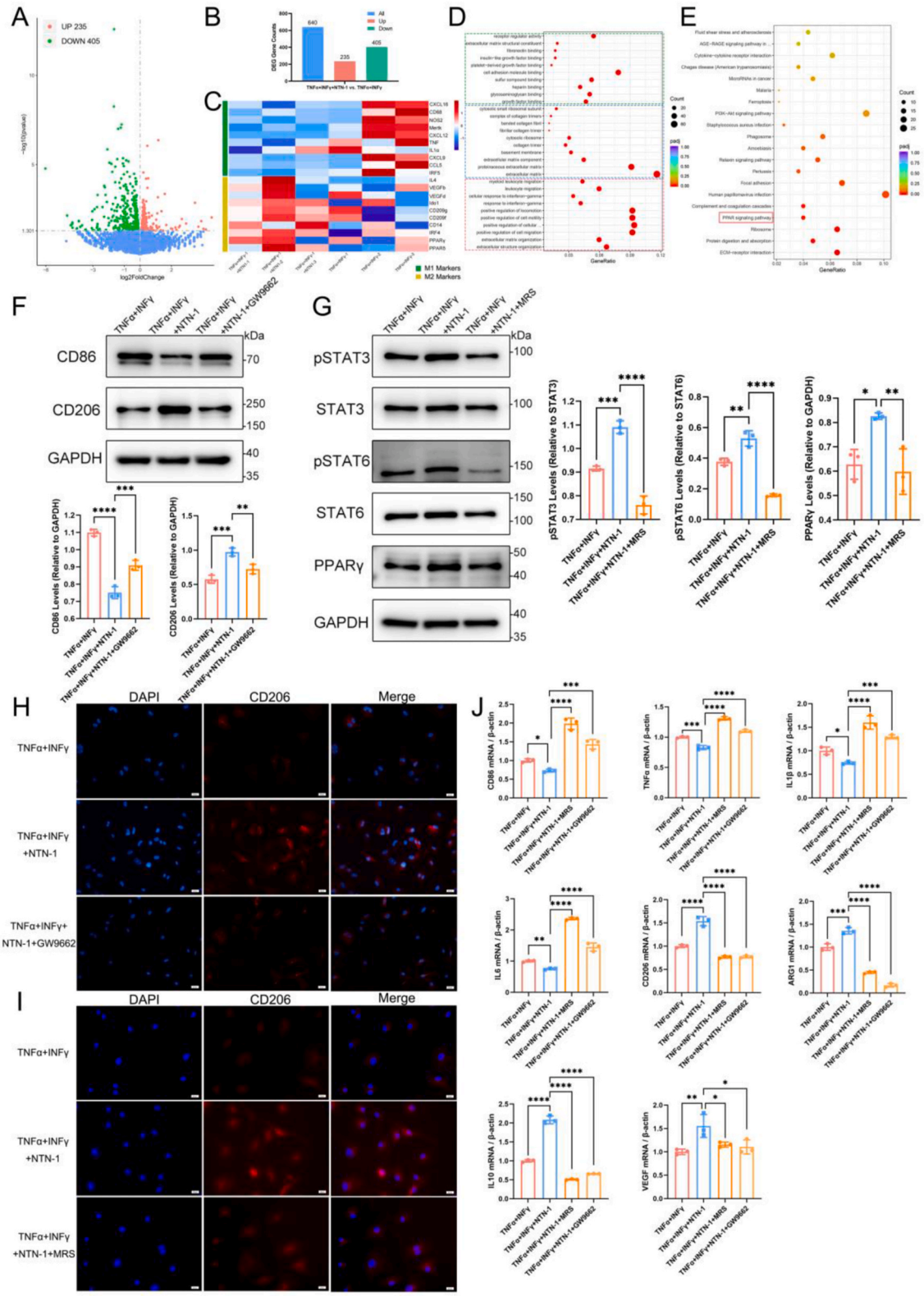

Fig. 4. Netrin-1 regulated macrophage polarization via the A2bR/STAT/PPARγ signaling pathway *in vitro*. (A) Volcano plot of the detected genes with 640 DEGs identified using the criteria (|log2 (fold change)|>0 and P < 0.05). (B) Histogram of the DEGs. (C) Heat map of the gene expression of M1 and M2 macrophage markers from the RNA-seq library (n = 3). (D–E) Gene ontology and Kyoto Encyclopedia of Genes and Genomes enrichment analyses. (F) Western blotting of CD86 and CD206 in netrin-1-treated macrophages upon exposure to GW9662 (n = 3). (G) Western blotting of the key proteins of the PPAR signaling pathway in netrin-1-treated macrophages upon MRS intervention (n = 3). (H–I) Immunofluorescence staining of CD206 showing the existing M2 phenotype (scale bar: 20 μm). (J) RT-qPCR analysis of macrophage markers (M1: CD86, TNF-α, IL-1β, and IL-6; M2: CD206, ARG1, IL-10, and VEGF) (n = 3). Netrin-1, NTN-1. Differentially expressed genes, DEGs. Data are shown as the mean ± SD. *P < 0.05, **P < 0.01, ***P < 0.001, and ****P < 0.0001.

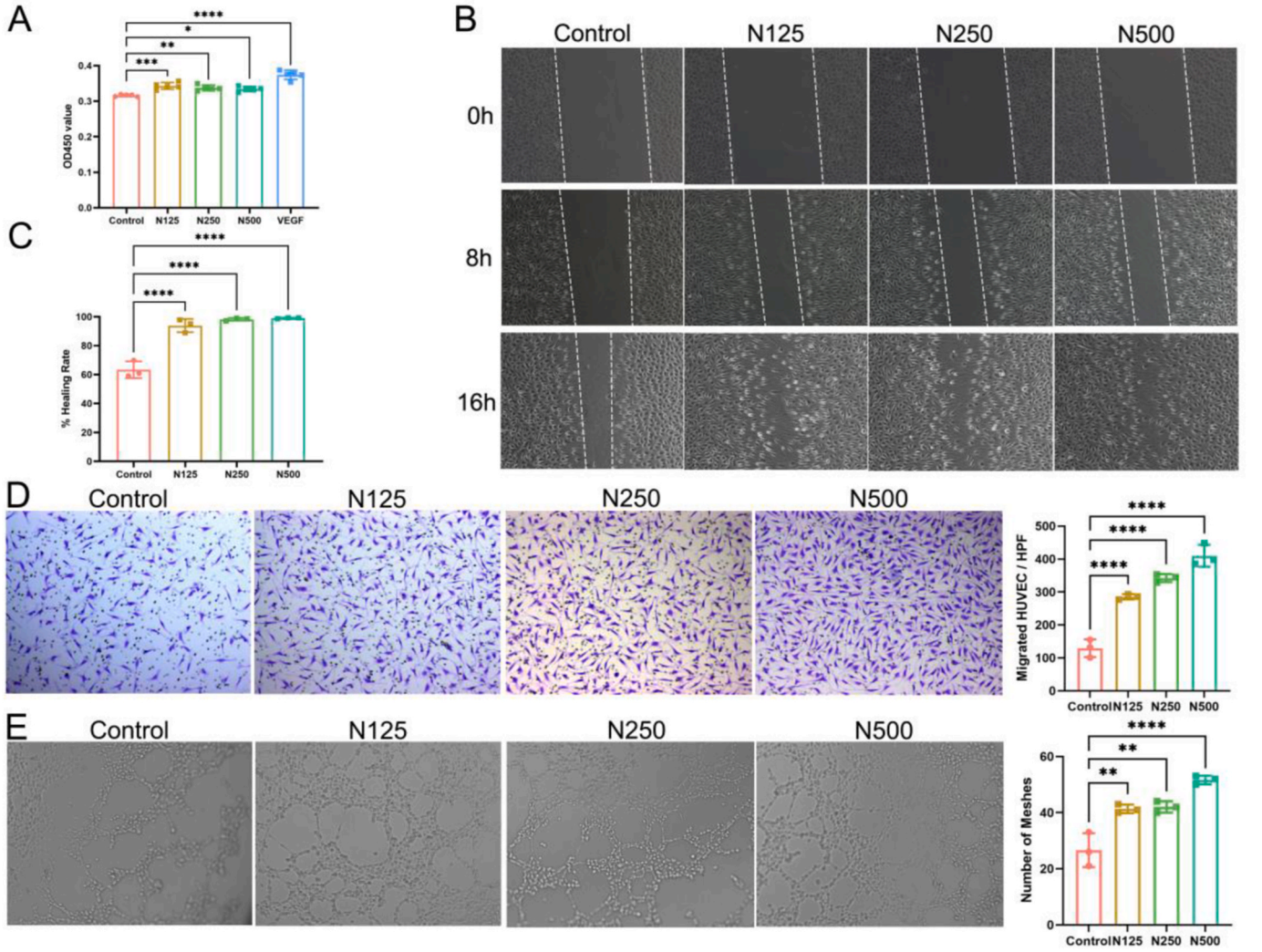

Fig. 5. Netrin-1 promoted the angiogenic capability of endothelial cells *in vitro*. (A) Results of the CCK-8 assay in HUVECs treated with netrin-1 (n = 5). (B–D) Results of the scratch and Transwell assays with statistical analyses showing the increased migration of HUVECs upon netrin-1 treatment (n = 3). (E) *In vitro* Matrigel tube formation of HUVECs with an analysis of the formed meshes (n = 3). Netrin-1 (125 ng/mL), N125; netrin-1 (250 ng/mL), N250; netrin-1 (500 ng/mL), N500. Data are shown as the mean ± SD. *P < 0.05, **P < 0.01, ***P < 0.001, and ****P < 0.0001.

indicating that netrin-1 may be involved in macrophage polarization during wound healing. We further discovered that netrin-1 expression in diabetic wounds remained abnormally lower on days 3 and 6 post-wounding than normal wounds. Previous studies have shown that macrophages could secrete Netrin-1 [36–39], and their accumulation during the inflammatory phase probably lays the foundation of the high expressions of netrin-1 in wound on day 3. However, the continuous hyperglycemia in the diabetic wound environment resulted in the impaired macrophages and may further inhibit netrin-1 secretion, thus finally generated the abnormal profile of sustaining low expression of netrin-1 in diabetic wounds. And local supplementation of netrin-1 *in vivo* and *in vitro* could promote macrophages to be a pro-healing phenotype and thus establish a favorable microenvironment. These results were verified using ELISA and RT-qPCR. As confirmed by the bioinformatics analysis and functional experiments performed in this study, the A2bR/STAT/PPARγ signaling pathway participated in macrophage polarization upon netrin-1 treatment, consistent with the previous reports [10,25,35].

As inflammation subsides, the wound healing process proceeds into the proliferation stage, characterized by robust angiogenesis, which supplies oxygen and nutrients to the cells, thus accelerating wound repair [6,40,41]. Endothelial cells exposed to persistent elevated blood glucose in diabetes have been evidenced to be dysfunctional with integrity loss, impaired angiogenesis and increased susceptibility to apoptosis, and the treatments rescuing microvascular dysfunction can significantly promote diabetic wound healing [6,41–43]. One study has reported that netrin-1 can prevent diabetes-induced vascular endothelial dysfunction in aorta and limit the reduction of NO level [44]. In addition, the adenovirus vector-mediated netrin-1 elevation in HUVECs up-regulated the PI3K/AKT-eNOS signaling pathway to restore the angiogenesis of endothelial cells, which was impaired by high glucose stimulation [45]. Accumulative evidences have presented the secretion of netrin-1 by endothelial cells [44–46]. In this study, we observed a sustained low profile of netrin-1 in diabetic wounds on day 6. A possible explanation for this might be the abnormal endothelial cells induced by persistent diabetic environment with the less netrin-1 secretion. And the local application of netrin-1 promoted neovascularization in diabetic wounds. This phenomenon can be explained by the direct and indirect effects of netrin-1 therapy. Firstly, we verified its direct efficacy through *in vitro* experiments, showing that netrin-1 could promote the proliferation, migration and angiogenic capability of endothelial cells. Moreover, TGF-β, IGF-1 and VEGF secreted by pro-healing M2 macrophages may promote angiogenesis indirectly.

It is of great importance to design an appropriate delivery system to

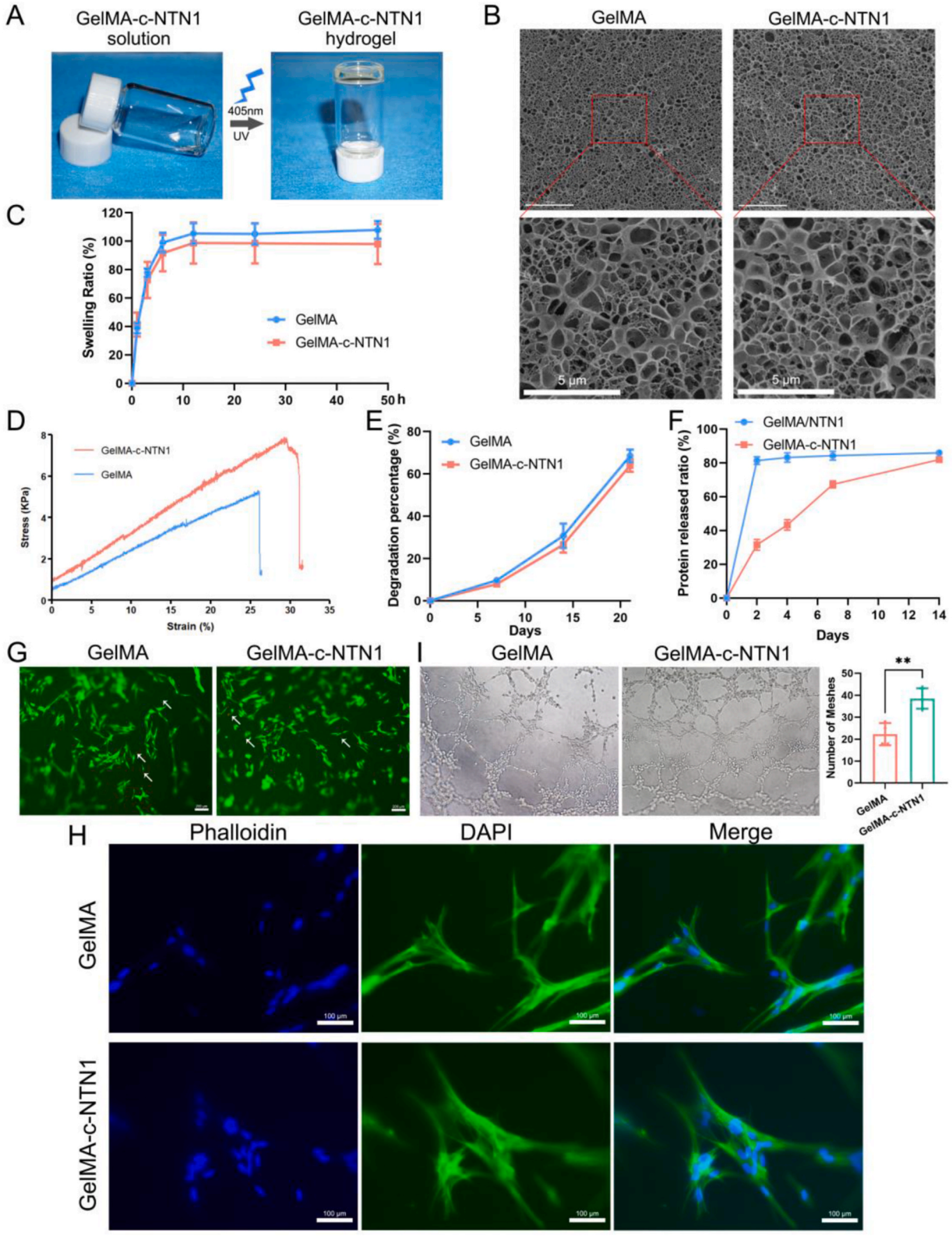

Fig. 6. Characterization, biocompatibility and bioactivity of the GelMA-*c*-NTN1 hydrogel. (A) Photograph of the GelMA-*c*-NTN1 solution and hydrogel formation after UV light exposure. (B) Scanning electron microscopy images of GelMA and GelMA-*c*-NTN1 (upper scale bar: 10 μm, lower scale bar: 5 μm). (C) Swelling ratio of GelMA and GelMA-*c*-NTN1 (n = 3). (D) Stress-strain curve of GelMA and GelMA-*c*-NTN1. (E) Degradation percentage of GelMA and GelMA-*c*-NTN1 over time (n = 3). (F) Protein release ratio of GelMA/NTN1 and GelMA-*c*-NTN1 (n = 3). (G) Live/dead staining of human fibroblasts (HFBs) cultured on GelMA and GelMA-*c*-NTN1 (white arrows: dead cells in red). (H) Phalloidin staining of the cytoskeleton of HFBs (scale bar: 100 μm). (I) Tube formation results of HUVECs (n = 3). Data are shown as the mean ± SD. **P < 0.01.

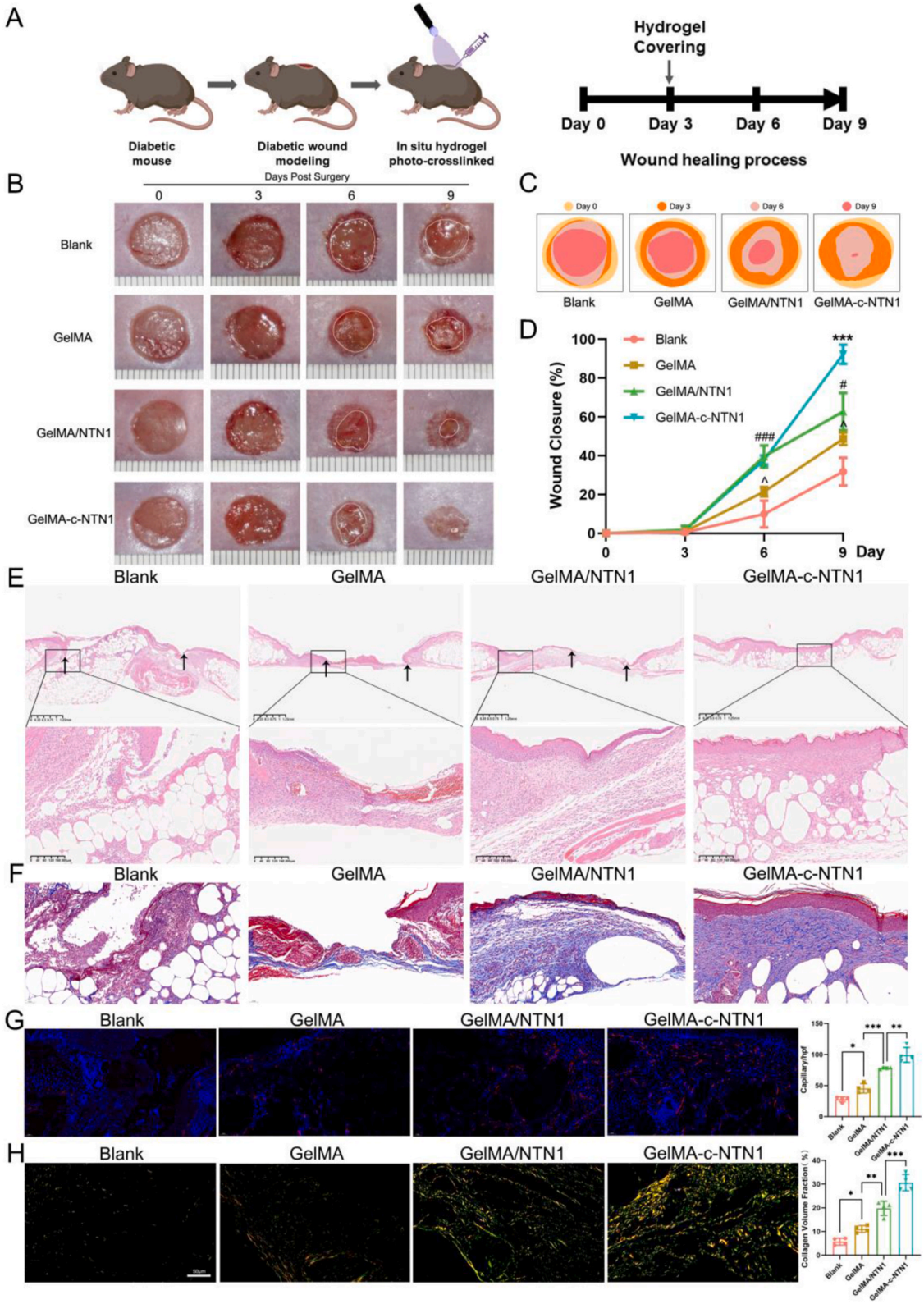

Fig. 7. GelMA-*c*-NTN1 hydrogel accelerated diabetic wound healing *in vivo*. (A) Schematic diagram of treating diabetic wounds using hydrogels. (B) Gross view of the wounds treated with phosphate-buffered saline (PBS; Blank), GelMA, GelMA/NTN1, and GelMA-*c*-NTN1. (C) Schematic diagrams of the wound areas over time. (D) Statistical analysis of the wound healing rates (%) (n = 4). (E) Hematoxylin and eosin staining of the wounds on day 9 post-wounding (upper scale bar: 1.25 mm, lower scale bar: 200 μm; black arrows indicate the wound edges). (F) The presentative images of Masson's trichrome staining (scale bar: 50 μm). (G) Immunofluorescence staining of CD31 with the corresponding statistical data (scale bar: 50 μm, n = 4). (H) Sirius Red staining with an analysis of collagen volume (scale bar: 50 μm, n = 4). Data are shown as the mean ± SD. * GelMA-*c*-NTN1 vs. GelMA/NTN1, # GelMA/NTN1 vs. GelMA, ^ GelMA vs. Blank. * or # or ^ $P < 0.05$, **$P < 0.01$, *** or ###$P < 0.001$.

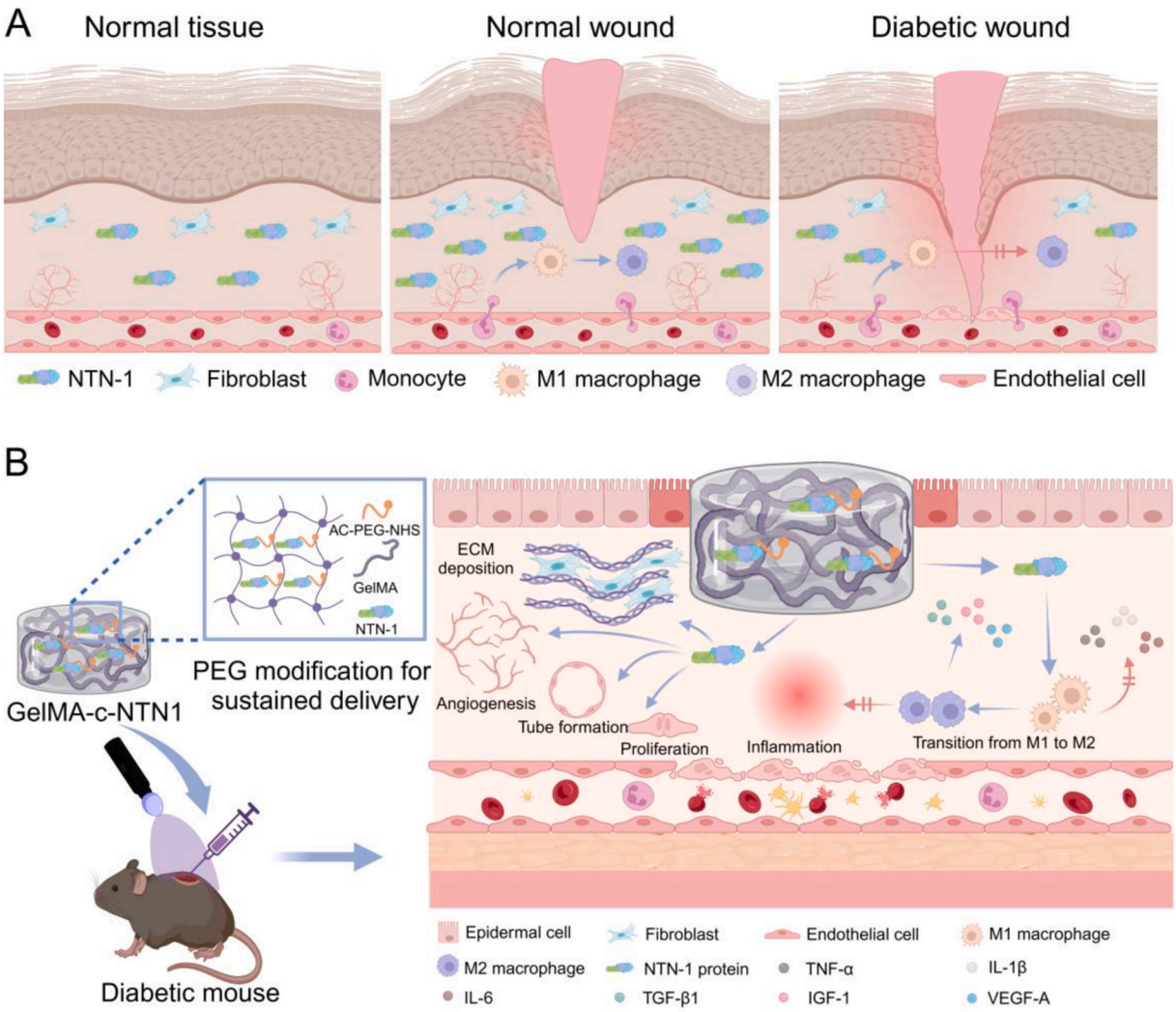

Fig. 8. Netrin-1 co-crosslinked hydrogel accelerated diabetic wound healing in situ. (A) Expression profiles of netrin-1 in normal tissue, normal wounds, and diabetic wounds. (B) Schematic diagram of the preparation of the GelMA-*c*-NTN1 hydrogel and its efficacy in healing diabetic wounds by modulating macrophage heterogeneity and promoting angiogenesis.

avoid injection pain and infection, and prolong the biological activity of netrin-1 in wounds [47–49]. Gelatin methacrylate (GelMA), a photopolymerizable and injectable hydrogel, is widely applied in tissue engineering and biomedical applications [50–54]. Researches have shown that GelMA hydrogels loaded with various active substances have excellent wound-healing promotion effects, and moreover, they have an extracellular matrix-like structure, good biocompatibility, biodegradability, and the ability to keep the wound moist [5,55–57]. These properties make the GelMA hydrogel highly suitable for the delivery of netrin-1 protein for diabetic wound treatment. However, GelMA mixed with soluble proteins via non-covalent interactions can cause a massive release of the active substance for a short time, leading to decreased protein bioavailability [58]. Previous studies have described the covalent immobilization of biomolecules with acrylate-PEG-NHS within a GelMA hydrogel for maintaining their natural bioactivity and achieving long-term release [58,59]. Using this sustained protein release system, we found that GelMA-*c*-NTN1 achieved much longer netrin-1 release than the GelMA hydrogel, while maintaining a multi-porous network, mechanical properties, degradability and biocompatibility similar to the GelMA hydrogel. When applied to diabetic wounds, the GelMA-*c*-NTN1 hydrogel showed faster wound healing efficacy than the GelMA, GelMA/NTN1 and control groups.

This study has some limitations. First, although the results indicated the direct contribution of the A2bR/STAT/PPARγ signaling pathway on macrophage polarization upon netrin-1 treatment, the data did not exclude the involvement of other signaling pathways. Second, other cells, such as keratinocytes and fibroblasts [4,60], are also important for wound healing. However, the effects of netrin-1 on these cells remain unknown and deserve further investigation.

5. Conclusions

In this study, we demonstrated the potential contribution of netrin-1 toward delayed wound healing in diabetes. Topical netrin-1 administration accelerated wound repair in diabetic mice, partially by promoting macrophage polarization towards the M2 phenotype via the A2bR/STAT/PPARγ signaling pathway and enhancing the angiogenic capability of endothelial cells. We further developed a GelMA-*c*-NTN1 hydrogel to achieve the sustained release of netrin-1 and this may provide a novel therapeutic approach for diabetic wound closure.

Ethics approval and consent to participate

The experimental protocol was performed in accordance with the ethical guidelines of the Helsinki Declaration and was approved by the Animal Ethics Committee of the First Affiliated Hospital of Naval

Medical University.

Data availability statement

Supporting data are available from the corresponding author upon reasonable request.

Formatting of funding sources

This work was supported by 173 plan project of Military Science and Technology (2019-JCJQ-ZD-359-00); the National Key R&D Program of China (2019YFA0110503, 2019YFA0110501); the National Nature Science Foundation of China (82072170, 82372512, 82172201, 82372513, 81930057 and 81701905); Shanghai Rising Star Program (22QA1411700); Basic medical research project of Changhai Hospital (2023YQ02); Changhong talent plan of Changhai Hospital; Youth Medical Talents -Specialist Program; Chinese Academy of Medical Sciences Innovation Fund for Medical Sciences (2019-I2M-5–076).

CRediT authorship contribution statement

Futing Shu: Writing – original draft, Visualization, Validation, Project administration, Methodology, Investigation, Formal analysis, Data curation. **Hongchao Huang:** Project administration, Methodology, Investigation, Formal analysis, Data curation. **Shichu Xiao:** Writing – review & editing, Supervision, Resources, Funding acquisition, Conceptualization. **Zhaofan Xia:** Writing – review & editing, Supervision, Resources, Funding acquisition, Conceptualization. **Yongjun Zheng:** Writing – review & editing, Visualization, Validation, Supervision, Resources, Funding acquisition, Conceptualization.

Declaration of competing interest

The authors declare that they have no known competing financial interests or personal relationships that could have appeared to influence the work reported in this paper.

Appendix A. Supplementary data

Supplementary data to this article can be found online at https://doi.org/10.1016/j.bioactmat.2024.04.019.

References

[1] H. Sun, P. Saeedi, S. Karuranga, M. Pinkepank, K. Ogurtsova, B.B. Duncan, C. Stein, A. Basit, J.C.N. Chan, J.C. Mbanya, M.E. Pavkov, A. Ramachandaran, S.H. Wild, S. James, W.H. Herman, P. Zhang, C. Bommer, S. Kuo, E.J. Boyko, D.J. Magliano, IDF Diabetes Atlas: global, regional and country-level diabetes prevalence estimates for 2021 and projections for 2045, Diabetes Res. Clin. Pract. 183 (2022) 109119.

[2] A.J. Boulton, L. Vileikyte, G. Ragnarson-Tennvall, J. Apelqvist, The global burden of diabetic foot disease, Lancet 366 (9498) (2005) 1719–1724.

[3] Y. Zheng, S. Zheng, X. Fan, L. Li, Y. Xiao, P. Luo, Y. Liu, L. Wang, Z. Cui, F. He, Y. Liu, S. Xiao, Z. Xia, Amniotic epithelial cells accelerate diabetic wound healing by modulating inflammation and promoting neovascularization, Stem Cell. Int. 2018 (2018) 1082076.

[4] B.R. Freedman, C. Hwang, S. Talbot, B. Hibler, S. Matoori, D.J. Mooney, Breakthrough treatments for accelerated wound healing, Sci. Adv. 9 (20) (2023) eade7007.

[5] Y.J. Fu, Y.F. Shi, L.Y. Wang, Y.F. Zhao, R.K. Wang, K. Li, S.T. Zhang, X.J. Zha, W. Wang, X. Zhao, W. Yang, All-natural immunomodulatory bioadhesive hydrogel promotes angiogenesis and diabetic wound healing by regulating macrophage heterogeneity, Adv. Sci. 10 (13) (2023) e2206771.

[6] Z. Shao, T. Yin, J. Jiang, Y. He, T. Xiang, S. Zhou, Wound microenvironment self-adaptive hydrogel with efficient angiogenesis for promoting diabetic wound healing, Bioact. Mater. 20 (2023) 561–573.

[7] X.P. Dun, D.B. Parkinson, Role of netrin-1 signaling in nerve regeneration, Int. J. Mol. Sci. 18 (3) (2017).

[8] J. Round, E. Stein, Netrin signaling leading to directed growth cone steering, Curr. Opin. Neurobiol. 17 (1) (2007) 15–21.

[9] Y. Sun, A. Manceau, L. Frydman, L. Cappuccio, D. Neves, V. Basso, H. Wang, J. Fombonne, C. Maisse, P. Mehlen, A. Paradisi, Delta40p53 isoform up-regulates netrin-1/UNC5B expression and potentiates netrin-1 pro-oncogenic activity, Proc. Natl. Acad. Sci. U. S. A. 118 (36) (2021).

[10] Y. Li, S. Wan, G. Liu, W. Cai, D. Huo, G. Li, M. Yang, Y. Wang, G. Guan, N. Ding, F. Liu, W. Zeng, C. Zhu, Netrin-1 promotes inflammation resolution to achieve endothelialization of small-diameter tissue engineering blood vessels by improving endothelial progenitor cells function in situ, Adv. Sci. 4 (12) (2017) 1700278.

[11] T. Tu, C. Zhang, H. Yan, Y. Luo, R. Kong, P. Wen, Z. Ye, J. Chen, J. Feng, F. Liu, J. Y. Wu, X. Yan, CD146 acts as a novel receptor for netrin-1 in promoting angiogenesis and vascular development, Cell Res. 25 (3) (2015) 275–287.

[12] G. Wu, Z. Wang, P. Shan, S. Huang, S. Lin, W. Huang, Z. Huang, Suppression of Netrin-1 attenuates angiotension II-induced cardiac remodeling through the PKC/MAPK signaling pathway, Biomed. Pharmacother. 130 (2020) 110495.

[13] Z. Wen, J.Q. Zheng, Directional guidance of nerve growth cones, Curr. Opin. Neurobiol. 16 (1) (2006) 52–58.

[14] J.M. van Gils, M.C. Derby, L.R. Fernandes, B. Ramkhelawon, T.D. Ray, K.J. Rayner, S. Parathath, E. Distel, J.L. Feig, J.I. Alvarez-Leite, A.J. Rayner, T.O. McDonald, K. D. O'Brien, L.M. Stuart, E.A. Fisher, A. Lacy-Hulbert, K.J. Moore, The neuroimmune guidance cue netrin-1 promotes atherosclerosis by inhibiting the emigration of macrophages from plaques, Nat. Immunol. 13 (2) (2012) 136–143.

[15] M. Schlegel, D. Kohler, A. Korner, T. Granja, A. Straub, M. Giera, V. Mirakaj, The neuroimmune guidance cue netrin-1 controls resolution programs and promotes liver regeneration, Hepatology 63 (5) (2016) 1689–1705.

[16] Y. Li, J.L. Chai, X. Shi, Y. Feng, J.J. Li, L.N. Zhou, C. Cao, K.R. Li, Galphai1/3 mediate Netrin-1-CD146-activated signaling and angiogenesis, Theranostics 13 (7) (2023) 2319–2336.

[17] B. Larrivee, C. Freitas, M. Trombe, X. Lv, B. Delafarge, L. Yuan, K. Bouvree, C. Breant, R. Del Toro, N. Brechot, S. Germain, F. Bono, F. Dol, F. Claes, C. Fischer, M. Autiero, J.L. Thomas, P. Carmeliet, M. Tessier-Lavigne, A. Eichmann, Activation of the UNC5B receptor by Netrin-1 inhibits sprouting angiogenesis, Genes Dev. 21 (19) (2007) 2433–2447.

[18] F. Shu, H. Gao, W. Wu, S. Yu, L. Zhang, H. Liu, S. Xiao, Z. Xia, Y. Zheng, Amniotic epithelial cells accelerate diabetic wound healing by protecting keratinocytes and fibroblasts from high-glucose-induced senescence, Cell Biol. Int. 46 (5) (2022) 755–770.

[19] D. Sticker, S. Lechner, C. Jungreuthmayer, J. Zanghellini, P. Ertl, Microfluidic migration and wound healing assay based on mechanically induced injuries of defined and highly reproducible areas, Anal. Chem. 89 (4) (2017) 2326–2333.

[20] K. Yamahara, T. Nakagawa, J. Ito, K. Kinoshita, K. Omori, N. Yamamoto, Netrin 1 mediates protective effects exerted by insulin-like growth factor 1 on cochlear hair cells, Neuropharmacology 119 (2017) 26–39.

[21] M. Sharifiaghdam, E. Shaabani, R. Faridi-Majidi, S.C. De Smedt, K. Braeckmans, J. C. Fraire, Macrophages as a therapeutic target to promote diabetic wound healing, Mol. Ther. 30 (9) (2022) 2891–2908.

[22] A.E. Louiselle, S.M. Niemiec, C. Zgheib, K.W. Liechty, Macrophage polarization and diabetic wound healing, Transl. Res. 236 (2021) 109–116.

[23] M. Rodrigues, N. Kosaric, C.A. Bonham, G.C. Gurtner, Wound healing: a cellular perspective, Physiol. Rev. 99 (1) (2019) 665–706.

[24] Y. Zheng, S. Ji, H. Wu, S. Tian, Y. Zhang, L. Wang, H. Fang, P. Luo, X. Wang, X. Hu, S. Xiao, Z. Xia, Topical administration of cryopreserved living micronized amnion accelerates wound healing in diabetic mice by modulating local microenvironment, Biomaterials 113 (2017) 56–67.

[25] Y. Zhang, P. Chen, G. Di, X. Qi, Q. Zhou, H. Gao, Netrin-1 promotes diabetic corneal wound healing through molecular mechanisms mediated via the adenosine 2B receptor, Sci. Rep. 8 (1) (2018) 5994.

[26] T.A. Wynn, K.M. Vannella, Macrophages in tissue repair, regeneration, and fibrosis, Immunity 44 (3) (2016) 450–462.

[27] M.L. Novak, T.J. Koh, Phenotypic transitions of macrophages orchestrate tissue repair, Am. J. Pathol. 183 (5) (2013) 1352–1363.

[28] H. Al Sadoun, Macrophage phenotypes in normal and diabetic wound healing and therapeutic interventions, Cells 11 (15) (2022).

[29] Y. Xiong, B.B. Mi, Z. Lin, Y.Q. Hu, L. Yu, K.K. Zha, A.C. Panayi, T. Yu, L. Chen, Z. P. Liu, A. Patel, Q. Feng, S.H. Zhou, G.H. Liu, The role of the immune microenvironment in bone, cartilage, and soft tissue regeneration: from mechanism to therapeutic opportunity, Mil Med Res 9 (1) (2022) 65.

[30] S. Patel, S. Srivastava, M.R. Singh, D. Singh, Mechanistic insight into diabetic wounds: pathogenesis, molecular targets and treatment strategies to pace wound healing, Biomed. Pharmacother. 112 (2019) 108615.

[31] Y. Xiong, Z. Lin, P. Bu, T. Yu, Y. Endo, W. Zhou, Y. Sun, F. Cao, G. Dai, Y. Hu, L. Lu, L. Chen, P. Cheng, K. Zha, M.A. Shahbazi, Q. Feng, B. Mi, G. Liu, A whole-course-repair system based on neurogenesis-angiogenesis crosstalk and macrophage reprogramming promotes diabetic wound healing, Adv. Mater. 35 (19) (2023) e2212300.

[32] X. Xia, Z. Hu, S. Wang, K. Yin, Netrin-1: an emerging player in inflammatory diseases, Cytokine Growth Factor Rev. 64 (2022) 46–56.

[33] M. Schlegel, M. Sharma, E.J. Brown, A.A.C. Newman, Y. Cyr, M.S. Afonso, E. M. Corr, G.J. Koelwyn, C. van Solingen, J. Guzman, R. Farhat, C.A. Nikain, L. C. Shanley, D. Peled, A.M. Schmidt, E.A. Fisher, K.J. Moore, Silencing myeloid netrin-1 induces inflammation resolution and plaque regression, Circ. Res. 129 (5) (2021) 530–546.

[34] X. Mao, H. Xing, A. Mao, H. Jiang, L. Cheng, Y. Liu, X. Quan, L. Li, Netrin-1 attenuates cardiac ischemia reperfusion injury and generates alternatively activated macrophages, Inflammation 37 (2) (2014) 573–580.

[35] P.V. Ranganathan, C. Jayakumar, G. Ramesh, Netrin-1-treated macrophages protect the kidney against ischemia-reperfusion injury and suppress inflammation by inducing M2 polarization, Am. J. Physiol. Ren. Physiol. 304 (7) (2013) F948–F957.

[36] R. Gao, X. Peng, C. Perry, H. Sun, A. Ntokou, C. Ryu, J.L. Gomez, B.C. Reeves, A. Walia, N. Kaminski, N. Neumark, G. Ishikawa, K.E. Black, L.P. Hariri, M. W. Moore, M. Gulati, R.J. Homer, D.M. Greif, H.K. Eltzschig, E.L. Herzog, Macrophage-derived netrin-1 drives adrenergic nerve-associated lung fibrosis, J. Clin. Invest. 131 (1) (2021).
[37] X. Guo, S. Ding, T. Li, J. Wang, Q. Yu, L. Zhu, X. Xu, G. Zou, Y. Peng, X. Zhang, Macrophage-derived netrin-1 is critical for neuroangiogenesis in endometriosis, Int. J. Biol. Macromol. 148 (2020) 226–237.
[38] T. Hadi, L. Boytard, M. Silvestro, D. Alebrahim, S. Jacob, J. Feinstein, K. Barone, W. Spiro, S. Hutchison, R. Simon, D. Rateri, F. Pinet, D. Fenyo, M. Adelman, K. J. Moore, H.K. Eltzschig, A. Daugherty, B. Ramkhelawon, Macrophage-derived netrin-1 promotes abdominal aortic aneurysm formation by activating MMP3 in vascular smooth muscle cells, Nat. Commun. 9 (1) (2018) 5022.
[39] B. Ramkhelawon, E.J. Hennessy, M. Menager, T.D. Ray, F.J. Sheedy, S. Hutchison, A. Wanschel, S. Oldebeken, M. Geoffrion, W. Spiro, G. Miller, R. McPherson, K. J. Rayner, K.J. Moore, Netrin-1 promotes adipose tissue macrophage retention and insulin resistance in obesity, Nat. Med. 20 (4) (2014) 377–384.
[40] L.A. DiPietro, Angiogenesis and wound repair: when enough is enough, J. Leukoc. Biol. 100 (5) (2016) 979–984.
[41] U.A. Okonkwo, L.A. DiPietro, Diabetes and wound angiogenesis, Int. J. Mol. Sci. 18 (7) (2017).
[42] J.Q. Yu, X.F. Liu, L.K. Chin, A.Q. Liu, K.Q. Luo, Study of endothelial cell apoptosis using fluorescence resonance energy transfer (FRET) biosensor cell line with hemodynamic microfluidic chip system, Lab Chip 13 (14) (2013) 2693–2700.
[43] Y. Zhang, M. Li, Y. Wang, F. Han, K. Shen, L. Luo, Y. Li, Y. Jia, J. Zhang, W. Cai, K. Wang, M. Zhao, J. Wang, X. Gao, C. Tian, B. Guo, D. Hu, Exosome/metformin-loaded self-healing conductive hydrogel rescues microvascular dysfunction and promotes chronic diabetic wound healing by inhibiting mitochondrial fission, Bioact. Mater. 26 (2023) 323–336.
[44] H.A. Toque, A. Fernandez-Flores, R. Mohamed, R.B. Caldwell, G. Ramesh, R. W. Caldwell, Netrin-1 is a novel regulator of vascular endothelial function in diabetes, PLoS One 12 (10) (2017) e0186734.
[45] Y. Xing, J. Lai, X. Liu, N. Zhang, J. Ming, H. Liu, X. Zhang, Netrin-1 restores cell injury and impaired angiogenesis in vascular endothelial cells upon high glucose by PI3K/AKT-eNOS, J. Mol. Endocrinol. 58 (4) (2017) 167–177.
[46] S. Renders, A.F. Svendsen, J. Panten, N. Rama, M. Maryanovich, P. Sommerkamp, L. Ladel, A.R. Redavid, B. Gibert, S. Lazare, B. Ducarouge, K. Schonberger, A. Narr, M. Tourbez, B. Dethmers-Ausema, E. Zwart, A. Hotz-Wagenblatt, D. Zhang, C. Korn, P. Zeisberger, A. Przybylla, M. Sohn, S. Mendez-Ferrer, M. Heikenwalder, M. Brune, D. Klimmeck, L. Bystrykh, P.S. Frenette, P. Mehlen, G. de Haan, N. Cabezas-Wallscheid, A. Trumpp, Niche derived netrin-1 regulates hematopoietic stem cell dormancy via its receptor neogenin-1, Nat. Commun. 12 (1) (2021) 608.
[47] J.B. Acosta, D.G. del Barco, D.C. Vera, W. Savigne, P. Lopez-Saura, G. Guillen Nieto, G.S. Schultz, The pro-inflammatory environment in recalcitrant diabetic foot wounds, Int. Wound J. 5 (4) (2008) 530–539.
[48] Y. Zhang, Y. Zheng, F. Shu, R. Zhou, B. Bao, S. Xiao, K. Li, Q. Lin, L. Zhu, Z. Xia, In situ-formed adhesive hyaluronic acid hydrogel with prolonged amnion-derived conditioned medium release for diabetic wound repair, Carbohydr. Polym. 276 (2022) 118752.
[49] B. Guo, Y. Liang, R. Dong, Physical dynamic double-network hydrogels as dressings to facilitate tissue repair, Nat. Protoc. 18 (11) (2023) 3322–3354.
[50] J.W. Nichol, S.T. Koshy, H. Bae, C.M. Hwang, S. Yamanlar, A. Khademhosseini, Cell-laden microengineered gelatin methacrylate hydrogels, Biomaterials 31 (21) (2010) 5536–5544.
[51] K. Yue, G. Trujillo-de Santiago, M.M. Alvarez, A. Tamayol, N. Annabi, A. Khademhosseini, Synthesis, properties, and biomedical applications of gelatin methacryloyl (GelMA) hydrogels, Biomaterials 73 (2015) 254–271.
[52] S. Xiao, T. Zhao, J. Wang, C. Wang, J. Du, L. Ying, J. Lin, C. Zhang, W. Hu, L. Wang, K. Xu, Gelatin methacrylate (GelMA)-Based hydrogels for cell transplantation: an effective strategy for tissue engineering, Stem Cell Rev Rep 15 (5) (2019) 664–679.
[53] W. Lu, M. Zeng, W. Liu, T. Ma, X. Fan, H. Li, Y. Wang, H. Wang, Y. Hu, J. Xie, Human urine-derived stem cell exosomes delivered via injectable GelMA templated hydrogel accelerate bone regeneration, Mater Today Bio 19 (2023) 100569.
[54] L. Ouyang, J.P.K. Armstrong, Q. Chen, Y. Lin, M.M. Stevens, Void-free 3D bioprinting for in-situ endothelialization and microfluidic perfusion, Adv. Funct. Mater. 30 (26) (2020) 1909009.
[55] N. Hu, Z. Cai, X. Jiang, C. Wang, T. Tang, T. Xu, H. Chen, X. Li, X. Du, W. Cui, Hypoxia-pretreated ADSC-derived exosome-embedded hydrogels promote angiogenesis and accelerate diabetic wound healing, Acta Biomater. 157 (2023) 175–186.
[56] S. Li, J. Sun, J. Yang, Y. Yang, H. Ding, B. Yu, K. Ma, M. Chen, Gelatin methacryloyl (GelMA) loaded with concentrated hypoxic pretreated adipose-derived mesenchymal stem cells(ADSCs) conditioned medium promotes wound healing and vascular regeneration in aged skin, Biomater. Res. 27 (1) (2023) 11.
[57] D. Yan, G. Cao, S. Mao, Z. Shang, C. Li, G. Zhou, X. Li, H. Xia, Y. Wang, Octopus -inspired gelatin-methacrylate scaffolds loaded with hBMSC-derived exosomes promote wound healing by regulating macrophage polarization, Smart Materials in Medicine 5 (1) (2024) 52–65.
[58] B.P. Mahadik, S. Pedron Haba, L.J. Skertich, B.A. Harley, The use of covalently immobilized stem cell factor to selectively affect hematopoietic stem cell activity within a gelatin hydrogel, Biomaterials 67 (2015) 297–307.
[59] B.V. Sridhar, N.R. Doyle, M.A. Randolph, K.S. Anseth, Covalently tethered TGF-beta 1 with encapsulated chondrocytes in a PEG hydrogel system enhances extracellular matrix production, J. Biomed. Mater. Res. 102 (12) (2014) 4464–4472.
[60] H.E. Talbott, S. Mascharak, M. Griffin, D.C. Wan, M.T. Longaker, Wound healing, fibroblast heterogeneity, and fibrosis, Cell Stem Cell 29 (8) (2022) 1161–1180.